Comparative Analysis of Frequency-Selective Wireless Power Transfer for Multiple-Rx Systems

Kisong Lee, *Member, IEEE*, and Sung Ho Chae, *Member, IEEE*

***Abstract*—In this article we describe a comparative study of the frequency-selective wireless power transfer (WPT) by considering two different configurations, Tx–Rx–Rx and Rx–Tx–Rx, in a multiple-receiver system. In this system, the receivers have different resonant frequencies and a transmitter can select a driving frequency to transfer power. Using an ECM, we analyze the power transfer efficiency (PTE) and the power distribution according to the variation of the driving frequency. We also find the achievable PTE ($\eta_{\max}$) and the maximum power division ratio ($\alpha_{\max}$) in numerical terms for both configurations. The analysis and experimental results provide insightful information for understanding the effects of the arrangement of the resonators on $\eta_{\max}$ and $\alpha_{\max}$ by comparison with the magnetic-resonant WPT, where the resonant frequencies of all the receivers are the same as the driving frequency. We find that the Rx–Tx–Rx configuration is generally more useful for distributing the power to the receivers than the Tx–Rx–Rx configuration, for both frequency-selective and magnetic-resonant WPT. In addition, the frequency-selective WPT enables a more adaptive power distribution than the magnetic-resonant WPT in the Rx–Tx–Rx configuration while maintaining $\eta_{\max}$. We further verify that the results of the analysis are in accordance with the measured values, by means of experiments conducted in a variety of environments.**

***Index Terms*—Equivalent circuit model (ECM), efficiency, frequency selectivity, power distribution, wireless power transfer (WPT).**

I. Introduction

With the recent development of electronic appliances, users are faced with the requirement to recharge the batteries of their devices increasingly, as a result of the rapid growth in levels of usage. To meet the ongoing demands to eliminate the need for wired power, the wireless power transfer (WPT) has emerged as a promising alternative. For the wireless charging of portable devices, medical appliances, and electric vehicles, technological advances in the WPT are expected to provide great benefits in terms of increased convenience for a broad variety of applications. Ever since the establishment of the magnetic-resonant WPT by Nikola Tesla in the last century [1], a number of authors have investigated the characteristics of the WPT [2]–[8]. In [2] and [3], the authors used the coupled mode theory to develop a theoretical analysis of the nonradiative WPT via strongly coupled magnetic resonance and presented the experimental verifications. In [4] and[5], the power transfer efficiency (PTE) was derived using an equivalent circuit model (ECM), and some optimal parameters were found, e.g., coupling coefficient and quality factor, to maximize the PTE. Furthermore, the optimal design of resonators were proposed to improve the PTE in [6]–[8].

The research on this topic has been extended to progressive WPT, including a multiple-transmitter (Tx) system [9]–[12], a relay system [13]–[18], and a multiple-receiver (Rx) system [19]–[24]. In the multiple-Tx system, the achievable PTE [9], the transmit diversity [10], [11], and the optimal activation and current ratio between Txs [12] were studied. In the relay system, the effects of relays on the performance improvement in the PTE [13], [14] and the stability [15] were investigated, together with the optimal placement of relays for the enhanced PTE [16]–[18]. In a variety studies of the multiple-Rx system, the adjustable power distribution [19]–[22], the means for compensating the cross coupling among Rxs [23], and the optimal configuration of Rxs [24] were all investigated. There were also several attempts to overcome the frequency splitting in order to enable reliable power transfer even in overcoupled regions [25]–[29], in which some authors suggested the possibility that the PTE could be improved by controlling the driving frequency [25], [27], [29]. Recently, the adaptive adjustment of the driving or resonant frequency was proposed as a means of improving the WPT performance even in situations where frequency splitting does not occur [30], [31]. In addition, the frequency-selective WPT has been considered to be a promising strategy for supporting multiple Rxs at the same time [32]–[36]. In particular, control methods [32], [33], [35] and circuit designs [34], [36] for tuning the driving or resonant frequency were proposed for transferring the power effectively to Rxs using multiple frequencies.

Previous work has provided a variety of analytical approaches and experimental results for enhancing the performance of the WPT for multiple-Rx systems [19]–[24], [32]–[36], but to the best of our knowledge, no study has suggested the comparative analysis of the frequency-selective WPT depending on the configuration of resonators in a multiple-Rx system. In this article,

Manuscript received May 13, 2019; revised August 10, 2019; accepted September 26, 2019. Date of publication October 1, 2019; date of current version February 11, 2020. The work of K. Lee was supported by the National Research Foundation of Korea (NRF) grant funded by the Korea government (MSIT) under Grant 2018R1C1B6003297 and the work of S. H. Chae was supported by the Research Grant of Kwangwoon University in 2019. Recommended for publication by Associate Editor Dr. M. Duffy. *(Corresponding author: Sung Ho Chae.)*

K. Lee is with the Department of Information and Communication Engineering, Dongguk University, Seoul 04620, Republic of Korea (e-mail: kslee851105@gmail.com).

S. H. Chae is with the Department of Electronic Engineering, Kwangwoon University, Seoul 01897, South Korea (e-mail: sho.chae00@gmail.com).

Color versions of one or more of the figures in this article are available online at http://ieeexplore.ieee.org.

Digital Object Identifier 10.1109/TPEL.2019.2944634

we consider multiple Rxs with different resonant frequencies, and present an ECM for the frequency-selective WPT, in which the driving frequency may differ from the resonant frequencies of the Rxs. We also provide an analysis of the performance of the frequency-selective WPT in terms of the achievable PTE and power distribution, and verify its accuracy through experiments. Our contributions can be summarized as follows.

1) We derive the general expression of the PTE for Tx–Rx–Rx and Rx–Tx–Rx configurations by introducing recursive notations in a WPT system with N Rxs. We also provided the achievable PTE and the maximum power division ratio for the frequency-selective WPT, which present the upper bounds on WPT performances in terms of the PTE and power distribution, respectively. From this result, it is shown that Rx–Tx–Rx configuration is more compatible for power distribution than the Tx–Rx–Rx configuration. In addition, by comparing the frequency-selective WPT with the magnetic-resonant WPT, we discover that it is advantageous to use the frequency-selective WPT to accomplish a higher achievable PTE for short distances in Tx–Rx–Rx configuration, rather than the magnetic-resonant WPT. Moreover, in the Rx–Tx–Rx configuration, it is preferable to use the frequency-selective WPT for distributing power among Rxs, compared with the magnetic-resonant WPT.
2) In order to verify the exactness of our analysis, we fabricate resonators with different resonant frequencies and perform experimental verifications under diverse environments. Due to a series of measurements undertaken using a vector network analyzer (VNA), we confirm the agreement between the analytical results and the measured data.
3) This is the first study to reveal the effect of the arrangement of resonators on the frequency-selective WPT performances including achievable PTE and power distribution, which is the novelty aspect of our findings. We anticipate that our study will provide insightful information on the selection of WPT methods and the configuration of resonators for improving the system efficiency as well as Rx fairness in a multiple-Rx system.

II. System Model

As shown in Fig. 1(a), we consider a frequency-selective WPT with a single Tx and two Rxs. According to the arrangement of the resonators, the WPT system is considered to be configured as Tx–Rx–Rx or Rx–Tx–Rx. The outer radius, the number of turns, and the pitch of the resonator i are defined as σ_i, τ_i, and ρ_i, respectively, where $i \in \{0, 1, 2\}$. Here, the subscript 0 indicates Tx, while the other subscripts $\{1, 2\}$ represent Rxs, respectively. The resonators are lined up along the same axis, and d_{ij} is the distance between the resonators i and j. Fig. 1(b) shows the transformer model of the WPT system considered. An alternating voltage source, V_S, and a source resistance, R_S, are connected to Tx 0, while a load resistor, $R_{L,i}$, is linked to Rx i. A self-inductance and a parasitic resistance for the resonator i are represented by L_i and r_i, respectively, and a lumped capacitance, C_i, is connected to the resonator i in series to give each

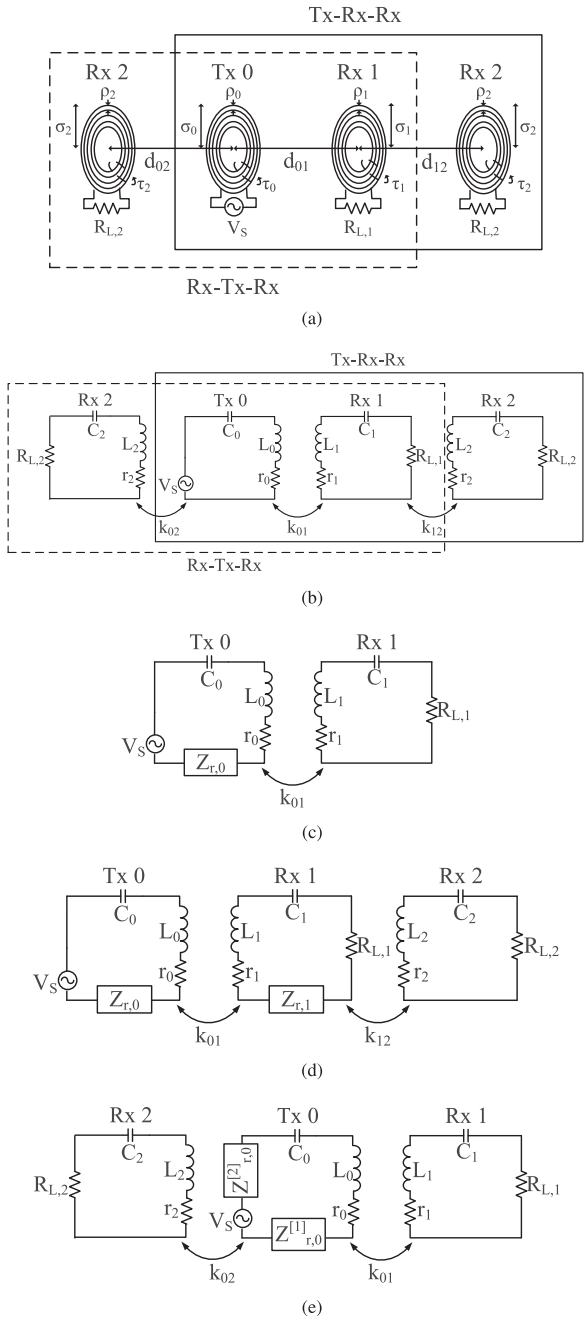

Fig. 1. Frequency-selective WPT with two receivers. (a) Resonator model. (b) Transformer model. (c) ECM for single Rx. (d) ECM for Tx–Rx–Rx. (e) ECM for Rx–Tx–Rx.

resonator its own resonant frequency. Thus, the resonant angular frequency of the resonator i is described as $\omega_i = 2\pi f_i = \frac{1}{\sqrt{L_i C_i}}$ for $i \in \{0, 1, 2\}$. The driving angular frequency, which is used for transferring the power at Tx, is denoted as $\omega = 2\pi f$.

Equivalent input impedances in Tx 0 and Rx i are given by

$$Z_0 = r_0 + j\omega L_0 - \frac{j}{\omega C_0} = r_0 + jX_0 \tag{1}$$

$$Z_i = R_{L,i} + r_i + j\omega L_i - \frac{j}{\omega C_i} = R_{L,i} + r_i + jX_i \tag{2}$$

where the reactance terms can be replaced by $X_i = \omega L_i - \frac{1}{\omega C_i}$ for $i \in \{0, 1, 2\}$. The strength of the magnetic link between two resonators i and j is expressed as a coupling coefficient, $k_{ij} = \frac{M_{ij}}{\sqrt{L_i L_j}}$, where M_{ij} is a mutual inductance and a reciprocal property is held, i.e., $k_{ij} = k_{ji}$ [16]–[18]. In addition, the cross-coupling between nonadjacent resonators can be negligible when they are sufficiently far apart [16]–[18], [24].

III. Frequency-Selective WPT

When Rxs have different resonant frequencies, they have different power transfer characteristics depending on the driving frequency. Therefore, in this section, we investigate the frequency-selective WPT for Rxs with different resonant frequencies in two different configurations, e.g., Tx–Rx–Rx and Rx–Tx–Rx, with respect to the achievable PTE and the power division ratio. In addition, we extend our analysis to the general case of the WPT with N Rxs.

A. Single Rx

First, we provide a brief description of a single-Rx system. To derive the PTE of the WPT system shown in Fig. 1(c), we use an ECM obtained by introducing a reflected impedance from Rx 1 to Tx 0 ($Z_{r,0}$), as follows:

$$Z_{r,0} = \frac{\omega^2 M_{01}^2}{R_{L,1} + r_1 + jX_1} \overset{(b)}{=} \frac{\omega^2 M_{01}^2 (R_{L,1} + r_1)}{(R_{L,1} + r_1)^2 + X_1^2}. \quad (3)$$

Note that the equality (b) comes from the fact that the power is not consumed in the reactance term X_1. Then, the PTE is

$$\eta_1 = \frac{Z_{r,0}}{r_0 + Z_{r,0}} \cdot \frac{R_{L,1}}{R_{L,1} + r_1} = \frac{k_{01}^2 Q_0 Q_1 F_1^2}{1 + k_{01}^2 Q_0 Q_1 F_1^2} \times \eta_{r,1} \quad (4)$$

where $Q_0 = \frac{\omega L_0}{r_0}$, $Q_1 = \frac{\omega L_1}{R_{L,1}+r_1}$, $F_1 = \frac{R_{L,1}+r_1}{\sqrt{(R_{L,1}+r_1)^2+X_1^2}}$, and $\eta_{r,1} = \frac{R_{L,1}}{R_{L,1}+r_1}$. Here, the quality factors of Tx 0 and Rx 1, Q_0 and Q_1, are an indication of the frequency selectivity of the resonant circuits, F_1 reflects how the driving frequency deviates from the resonant frequency of Rx 1, and $\eta_{r,1}$ is the circuit efficiency of Rx 1. In addition, $F_0 = \frac{r_0}{\sqrt{r_0^2+X_0^2}}$ represents the amount of the driving frequency that deviates from the resonant frequency of Tx 0. From (4), it is observed that η_1 is affected only by F_1, and not by F_0. This indicates that the discrepancy between the driving frequency and the resonant frequency of Tx has no influence on the PTE. In addition, F_1^2 becomes a value of 1 when the driving frequency is the same as the resonant frequency of Rx 1, i.e., $\omega = \omega_1$, because the reactance term X_1 becomes zero. Therefore, in the magnetic-resonant WPT where $\omega = \omega_1$, η_1 is transformed to

$$\eta_1 = \frac{k_{01}^2 Q_0 Q_1}{1 + k_{01}^2 Q_0 Q_1} \times \eta_{r,1}. \quad (5)$$

In (5), η_1 is proportional to k_{01}, $Q_0 Q_1$, and $\eta_{r,1}$. This means that the PTE can be improved in the following conditions:

1) the resonators are strongly coupled (e.g., higher k_{01});
2) the resonators are designed to have a higher quality factor (e.g., higher $Q_0 Q_1$);
3) Rx 1 has a higher circuit efficiency with a lower internal resistance (e.g., higher $\eta_{r,1}$).

B. Tx–Rx–Rx Configuration

We consider Tx–Rx–Rx configuration where the Rxs are located on one side of Tx, in order to analyze the nature of the power division at Rxs that have different resonant frequencies; the aim is also to determine the achievable PTE.[1] As shown in Fig. 1(d), the reflected impedance from Rx 2 to Rx 1, $Z_{r,1}$, and the reflected impedance from Rx 1 to Tx 0, $Z_{r,0}$, can be represented by

$$Z_{r,1} = \frac{\omega^2 M_{12}^2}{R_{L,2}+r_2+jX_2} = \frac{\omega^2 M_{12}^2 (R_{L,2}+r_2)}{(R_{L,2}+r_2)^2+X_2^2} \quad (6)$$

$$Z_{r,0} = \frac{\omega^2 M_{01}^2}{R_{L,1}+r_1+jX_1+Z_{r,1}} = \frac{\omega^2 M_{01}^2 (R_{L,1}+r_1+Z_{r,1})}{(R_{L,1}+r_1+Z_{r,1})^2+X_1^2}. \quad (7)$$

Then, the PTE at each Rx is found from (8) and (9) shown at the bottom of this page, where $Q_i = \frac{\omega L_i}{R_{L,i}+r_i}$, $F_i = \frac{R_{L,i}+r_i}{\sqrt{(R_{L,i}+r_i)^2+X_i^2}}$, and $\eta_{r,i} = \frac{R_{L,i}}{R_{L,i}+r_i}$ for Rx i.

In (9), it is observed that the factors related to Rx 1, $k_{01}^2 Q_0 Q_1 F_1^2$, have a considerable effect on η_2 because Rx 1 and Rx 2 are arranged in a row. From this result, we note that Rx 2 suffers a severe loss of the PTE, because most of the power is transferred to Rx 1, which is close to Tx 0 in the Tx–Rx–Rx

[1]Note that the magnetic coupling between resonators can be formulated by a coupling coefficient, k_{ij}, whether the centers of resonators are aligned or not [37], [38]. Therefore, Rxs do not need to be placed in a line for Tx–Rx–Rx and Rx–Tx–Rx configurations as long as the ignorance of cross coupling is satisfied.

$$\eta_1 = \frac{Z_{r,0}}{r_0 + Z_{r,0}} \frac{R_{L,1}}{R_{L,1} + r_1 + Z_{r,1}} = \frac{k_{01}^2 Q_0 Q_1 F_1^2}{1 + k_{01}^2 Q_0 Q_1 F_1^2 (1 + k_{12}^2 Q_1 Q_2 F_2^2) + k_{12}^2 Q_1 Q_2 F_1^2 F_2^2 (2 + k_{12}^2 Q_1 Q_2 F_2^2)} \times \eta_{r,1} \quad (8)$$

$$\eta_2 = \frac{Z_{r,0}}{r_0 + Z_{r,0}} \frac{Z_{r,1}}{R_{L,1} + r_1 + Z_{r,1}} \frac{R_{L,2}}{R_{L,2} + r_2} = \frac{k_{01}^2 k_{12}^2 Q_0 Q_1^2 Q_2 F_1^2 F_2^2}{1 + k_{01}^2 Q_0 Q_1 F_1^2 (1 + k_{12}^2 Q_1 Q_2 F_2^2) + k_{12}^2 Q_1 Q_2 F_1^2 F_2^2 (2 + k_{12}^2 Q_1 Q_2 F_2^2)} \times \eta_{r,2} \quad (9)$$

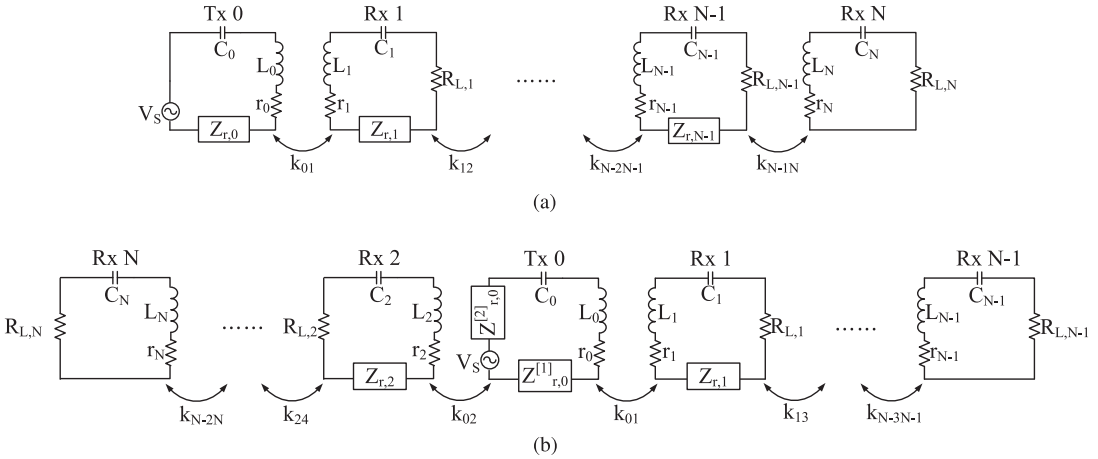

Fig. 2. Frequency-selective WPT with N receivers. (a) ECM for Tx–Rx–Rx with N Rxs. (b) ECM for Rx–Tx–Rx with N Rxs.

configuration. The overall PTE of the WPT system can also be expressed as the sum of η_1 and η_2, as (10) shown at the bottom of this page.

The ratio of the PTE between Rx 1 and Rx 2 can also be described as

$$k_{01}^2 Q_0 Q_1 F_1^2 \eta_{r,1} : k_{01}^2 k_{12}^2 Q_0 Q_1^2 Q_2 F_1^2 F_2^2 \eta_{r,2} = 1 : \alpha. \quad (11)$$

The maximum power division ratio, $\alpha_{\max}$, can be found as

$$\alpha_{\max} = \max_{\omega} k_{12}^2 Q_1 Q_2 F_2^2 \frac{\eta_{r,2}}{\eta_{r,1}}. \quad (12)$$

Here, it is confirmed that $\alpha_{\max}$ is observed near the resonant frequency of Rx 2 because F_2^2 becomes 1 at $\omega = \omega_2$. However, we expect the adaptive power division for Rxs to be difficult in the Tx–Rx–Rx configuration because the term $k_{12}^2 Q_1 Q_2 F_2^2$ restricts the increase in $\alpha_{\max}$.

The results can be extended to the WPT system with N Rxs, as shown in Fig. 2(a). The reflected impedance from Rx $i+1$ to the resonator i, $Z_{r,i}$, is represented by

$$\begin{aligned} Z_{r,i} &= \frac{\omega^2 M_{i(i+1)}^2}{R_{L,i+1} + r_{i+1} + jX_{i+1} + Z_{r,i+1}} \\ &= \frac{\omega^2 M_{i(i+1)}^2 (R_{L,i+1} + r_{i+1} + Z_{r,i+1})}{(R_{L,i+1} + r_{i+1} + Z_{r,i+1})^2 + X_{i+1}^2}. \end{aligned} \quad (13)$$

In addition, to express η_i as a function of the coupling coefficient and quality factor, we introduce the following recursive notation:

$$\tilde{\zeta}_i = 1 + \cfrac{k_{(i-1)i}^2 Q_{i-1} Q_i \tilde{F}_i^2}{1 + \cfrac{k_{i(i+1)}^2 Q_i Q_{i+1} \tilde{F}_{i+1}^2}{1 + \cfrac{k_{(i+1)(i+2)}^2 Q_{i+1} Q_{i+2} \tilde{F}_{i+2}^2}{\ddots \over 1 + k_{(N-1)N}^2 Q_{N-1} Q_N \tilde{F}_N^2}}}$$

$$= 1 + \cfrac{\tilde{\beta}_i}{1 + \cfrac{\tilde{\beta}_{i+1}}{1 + \cfrac{\tilde{\beta}_{i+2}}{\ddots \over 1 + \tilde{\beta}_N}}}$$

$$= 1 + \frac{\tilde{\beta}_i}{\tilde{\zeta}_{i+1}}, \text{ for } i \in \{1, 2, \ldots, N\}. \quad (14)$$

In (14), $\tilde{F}_i = \frac{R_{L,i} + r_i + Z_{r,i}}{\sqrt{(R_{L,i} + r_i + Z_{r,i})^2 + X_i^2}}$ for $i \in \{1, 2, \ldots, N-1\}$, while $\tilde{F}_N = F_N = \frac{R_{L,N} + r_N}{\sqrt{(R_{L,N} + r_N)^2 + X_N^2}}$, and $\tilde{\beta}_i = k_{(i-1)i}^2 Q_{i-1} Q_i \tilde{F}_i^2$ for $i \in \{1, 2, \ldots, N\}$. Using the recursive notation $\tilde{\zeta}_i$, the PTE at Rx i is represented by

$$\begin{aligned} \eta_i &= \left(\frac{Z_{r,0}}{r_0 + Z_{r,0}}\right) \left(\prod_{j=1}^{i-1} \frac{Z_{r,j}}{R_{L,j} + r_j + Z_{r,j}}\right) \left(\frac{R_{L,i}}{R_{L,i} + r_i + Z_{r,i}}\right) \\ &= \left(\prod_{j=1}^{i} \frac{\tilde{\zeta}_j - 1}{\tilde{\zeta}_j}\right) \left(\frac{\eta_{r,i}}{\tilde{\zeta}_{i+1}}\right) \end{aligned} \quad (15)$$

where $Z_{r,N} = 0$ and $\tilde{\zeta}_{N+1} = 1$. In (15), it is observed that η_i decreases as i increases because $\frac{\tilde{\zeta}_j - 1}{\tilde{\zeta}_j} < 1$. From this fact, we note that an Rx that is further away from Tx achieves a lower PTE. Moreover, from the fact that $\tilde{\zeta}_j$ is proportional to the coupling coefficient and quality factor of the resonators, we confirm that the PTE at each Rx can be improved when the adjacent resonators are strongly coupled (e.g., higher k), and the resonators are fabricated with a higher quality factor (e.g., higher Q).

$$\eta = \frac{k_{01}^2 Q_0 Q_1 F_1^2 (\eta_{r,1} + k_{12}^2 Q_1 Q_2 F_2^2 \eta_{r,2})}{1 + k_{01}^2 Q_0 Q_1 F_1^2 (1 + k_{12}^2 Q_1 Q_2 F_2^2) + k_{12}^2 Q_1 Q_2 F_1^2 F_2^2 (2 + k_{12}^2 Q_1 Q_2 F_2^2)} \quad (10)$$

The overall PTE can be expressed as

$$\eta = \sum_{i=1}^{N} \eta_i = \sum_{i=1}^{N} \left(\prod_{j=1}^{i} \frac{\tilde{\zeta}_j - 1}{\tilde{\zeta}_j} \right) \left(\frac{\eta_{r,i}}{\tilde{\zeta}_{i+1}} \right). \tag{16}$$

In addition, the achievable PTE can be found by optimizing the driving frequency to that at which the maximum PTE can be achieved, as follows:

$$\eta_{\max} = \max_{\omega} \eta. \tag{17}$$

In the magnetic-resonant WPT, $\tilde{F}_i$ becomes 1 because the resonant frequencies of all the Rxs are the same as the driving frequency, i.e., $\omega = \omega_i$ for $i \in \{1, 2, \ldots, N\}$. Then, the achievable PTE can be transformed to

$$\eta_{\max} = \sum_{i=1}^{N} \left(\prod_{j=1}^{i} \frac{\zeta_j - 1}{\zeta_j} \right) \left(\frac{\eta_{r,i}}{\zeta_{i+1}} \right). \tag{18}$$

Here, ζ_i is defined as $\zeta_i = 1 + \frac{\beta_i}{\zeta_{i+1}}$, where $\beta_i = k_{(i-1)i}^2 Q_{i-1} Q_i$ for $i \in \{1, 2, \ldots, N\}$.

C. Rx–Tx–Rx Configuration

We regard Rx–Tx–Rx configuration, in which the Rxs are placed on both sides of Tx, as shown in Fig. 1(e). Similar to the Tx–Rx–Rx configuration, the reflected impedances from Rx 1 and Rx 2 to Tx 0, $Z_{r,0}^{[1]}$ and $Z_{r,0}^{[2]}$, are expressed as

$$Z_{r,0}^{[1]} = \frac{\omega^2 M_{01}^2}{R_{L,1} + r_1 + jX_1} = \frac{\omega^2 M_{01}^2 (R_{L,1} + r_1)}{(R_{L,1} + r_1)^2 + X_1^2} \tag{19}$$

$$Z_{r,0}^{[2]} = \frac{\omega^2 M_{02}^2}{R_{L,2} + r_2 + jX_2} = \frac{\omega^2 M_{02}^2 (R_{L,2} + r_2)}{(R_{L,2} + r_2)^2 + X_2^2}. \tag{20}$$

Then, the PTE at each Rx is obtained as

$$\begin{aligned} \eta_1 &= \frac{Z_{r,0}^{[1]}}{r_0 + Z_{r,0}^{[1]} + Z_{r,0}^{[2]}} \cdot \frac{R_{L,1}}{R_{L,1} + r_1} \\ &= \frac{k_{01}^2 Q_0 Q_1 F_1^2}{1 + k_{01}^2 Q_0 Q_1 F_1^2 + k_{02}^2 Q_0 Q_2 F_2^2} \times \eta_{r,1} \end{aligned} \tag{21}$$

$$\begin{aligned} \eta_2 &= \frac{Z_{r,0}^{[2]}}{r_0 + Z_{r,0}^{[1]} + Z_{r,0}^{[2]}} \cdot \frac{R_{L,2}}{R_{L,2} + r_2} \\ &= \frac{k_{02}^2 Q_0 Q_2 F_2^2}{1 + k_{01}^2 Q_0 Q_1 F_1^2 + k_{02}^2 Q_0 Q_2 F_2^2} \times \eta_{r,2}. \end{aligned} \tag{22}$$

From (21) and (22), we confirm that each Rx has a relatively low impact on the PTE of the other Rx, compared to the Tx–Rx–Rx configuration. In addition, the Rx, which has a higher coupling coefficient, quality factor, and circuit efficiency, can achieve a higher PTE than the other Rx. The overall PTE of the WPT system can be expressed as the sum of η_1 and η_2, as follows:

$$\eta = \frac{k_{01}^2 Q_0 Q_1 F_1^2 \eta_{r,1} + k_{02}^2 Q_0 Q_2 F_2^2 \eta_{r,2}}{1 + k_{01}^2 Q_0 Q_1 F_1^2 + k_{02}^2 Q_0 Q_2 F_2^2}. \tag{23}$$

The ratio of the PTE between Rx 1 and Rx 2 is given by

$$k_{01}^2 Q_0 Q_1 F_1^2 \eta_{r,1} : k_{02}^2 Q_0 Q_2 F_2^2 \eta_{r,2} = 1 : \alpha. \tag{24}$$

In the aforementioned equation, F_1^2 becomes 1, while F_2^2 has a much larger value at $\omega = \omega_1$, and vice versa at $\omega = \omega_0$. Therefore, the power can be adjustably transferred to the Rxs by controlling the driving frequency. Moreover, the maximum power division ratio, $\alpha_{\max}$, is expressed as

$$\alpha_{\max} = \max_{\omega} \frac{k_{02}^2 Q_2 F_2^2 \eta_{r,2}}{k_{01}^2 Q_1 F_1^2 \eta_{r,1}}. \tag{25}$$

Unlike the Tx–Rx–Rx configuration, $\alpha_{\max}$ can have a much larger value because it depends only on the ratio of $k_{01}^2 Q_1 F_1^2 \eta_{r,1}$ and $k_{02}^2 Q_2 F_2^2 \eta_{r,2}$.

The results can be extended to a WPT system with N Rxs. As shown in Fig. 2(b), we use odd numbers, e.g., $\{1, 3, \ldots, N-1\}$, to denote the Rxs on the right-hand side of Tx and even numbers, e.g., $\{2, 4, \ldots, N\}$, to represent the Rxs on the left-hand side of Tx. The reflected impedance from Rx $i+2$ to Rx i, $Z_{r,i}$, is represented by

$$\begin{aligned} Z_{r,i} &= \frac{\omega^2 M_{i(i+2)}^2}{R_{L,i+2} + r_{i+2} + jX_{i+2} + Z_{r,i+2}} \\ &= \frac{\omega^2 M_{i(i+2)}^2 (R_{L,i+2} + r_{i+2} + Z_{r,i+2})}{(R_{L,i+2} + r_{i+2} + Z_{r,i+2})^2 + X_{i+2}^2} \end{aligned} \tag{26}$$

where $i \in \{1, 2, \ldots, N-2\}$. To express the PTE at each Rx as a function of the coupling coefficient and quality factor, we introduce the following recursive notation:

$$\begin{aligned} \tilde{\zeta}_i &= 1 + \cfrac{k_{(i-2)i}^2 Q_{i-2} Q_i \tilde{F}_i^2}{1 + \cfrac{k_{i(i+2)}^2 Q_i Q_{i+2} \tilde{F}_{i+2}^2}{1 + \cfrac{k_{(i+2)(i+4)}^2 Q_{i+2} Q_{i+4} \tilde{F}_{i+4}^2}{\ddots \cfrac{}{1 + k_{(N-2)N}^2 Q_{N-2} Q_N \tilde{F}_N^2}}}} \\ &= 1 + \cfrac{\tilde{\beta}_i}{1 + \cfrac{\tilde{\beta}_{i+2}}{1 + \cfrac{\tilde{\beta}_{i+4}}{\ddots \cfrac{}{1 + \tilde{\beta}_N}}}} \\ &= 1 + \frac{\tilde{\beta}_i}{\tilde{\zeta}_{i+2}}, \text{ for } i \in \{1, 2, \ldots, N\}. \end{aligned} \tag{27}$$

where $\tilde{\beta}_i = k_{(i-2)i}^2 Q_{i-2} Q_i \tilde{F}_i^2$, $\tilde{F}_{N-1} = F_{N-1}$, $\tilde{F}_N = F_N$, $k_{(-1)1} = k_{01}$, and $Q_{-1} = Q_0$. Then, the PTEs at Rx $(2i-1)$ and Rx $2i$ are represented by the following equations, where $Z_{r,N-1} = Z_{r,N} = 0$ and $\tilde{\zeta}_{N+1} = \tilde{\zeta}_{N+2} = 1$. Similar to (15), we can confirm that a higher coupling coefficient and quality factor guarantee a higher PTE from (28) and (29) shown at the bottom of next page.

The overall PTE can be expressed as (30) shown at the bottom of next page. Moreover, the achievable PTE can be written as

$$\eta_{\max} = \max_{\omega} \eta. \tag{31}$$

In the magnetic-resonant WPT, $\tilde{F}_i = 1$ at $\omega = \omega_i$ for $i \in \{1, 2, \ldots, N\}$, thus the achievable PTE can be derived as (32) shown at the bottom of this page, in which ζ_i is defined as $\zeta_i = 1 + \frac{\beta_i}{\zeta_{i+2}}$ and $\beta_i = k^2_{(i-2)i} Q_{i-2} Q_i$, for $i \in \{1, 2, \ldots, N\}$.

IV. Experimental Results and Discussion

In order to verify our results by experimental means, we fabricated resonators with a spiral shape using the Litz wire. All the resonators had an identical structure, and their specifications were as follows: $\sigma = 15$ cm, $\rho = 0.5$ cm, $\tau = 3$, $L = 7.4$ μH, $r = 2.7$ Ω, and $R_L = 50$ Ω. We also made the resonators to have different frequencies by adjusting capacitance in each case. For example, the capacitances connected to Tx 0, Rx 1, and Rx 2 were $C_0 = 86.8$ pF, $C_1 = 74.5$ pF, and $C_2 = 64.6$ pF in series, thus giving resonant frequencies of $f_0 = 6.28$ MHz, $f_1 = 6.78$ MHz, and $f_2 = 7.28$ MHz, respectively. We also showed experimental results for a multiple-Rx system obtained by increasing the number of Rxs up to $N = 6$. An example of the experimental setup for $N = 4$ is shown in Fig. 3. Based on this experimental setup, we measured scattering parameters including S_{00} and S_{i0} for $i \in \{1, 2, \ldots, N\}$ using a vector network analyzer (Agilent E8357 A), and calculated the overall PTE as follows [23]:[2]

$$\eta = \frac{\sum_1^N |S_{i0}|^2}{1 - |S_{00}|^2}. \tag{33}$$

Fig. 4 shows the PTE (η) versus the driving frequency (f); (a) for the Tx–Rx–Rx configuration when $d_{01} = d_{12} = 30$ cm and

[2]Note that S_{00} indicates the input port voltage reflection coefficient for Tx 0, while S_{i0} represents the forward voltage gains for Rx i.

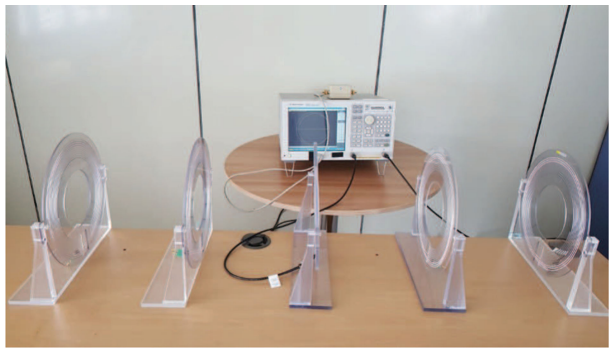

Fig. 3. Example of experimental setup for Rx–Tx–Rx when $N = 4$.

(b) for the Rx–Tx–Rx configuration when $d_{01} = d_{02} = 30$ cm. Here, the lines represent the analytical results (Ana.), while the hollow markers indicate the experimental results (Exp.). In Tx–Rx–Rx, Rx 1 and Rx 2 achieve a maximum PTE near their own resonant frequencies, e.g., $\eta_1 = 0.46$ at $f = 6.8$ MHz and $\eta_2 = 0.02$ at $f = 7.2$ MHz, respectively. Here, most of the power is transferred to the nearer Rx, therefore, η_1 has a considerable influence on the overall PTE, η. As a result, the achievable PTE occurs near the resonant frequency of Rx 1, e.g., $\eta_{\max} = 0.48$ at $f = 6.8$ MHz. Similar to Tx–Rx–Rx, in Rx–Tx–Rx each Rx achieves a maximum PTE near its own resonant frequency, e.g., $\eta_1 = 0.38$ at $f = 6.7$ MHz and $\eta_2 = 0.39$ at $f = 7.4$ MHz. However, both Rxs receive a similar amount of power from Tx, so η_1 and η_2 have a similar influence on η. In consequence, the achievable PTE is observed at a frequency between f_1 and f_2, e.g., $\eta_{\max} = 0.61$ at $f = 7.1$ MHz. In addition, we confirm

$$\begin{aligned}
\eta_{2i-1} &= \left(\frac{Z^{[1]}_{r,0}}{r_0 + Z^{[1]}_{r,0} + Z^{[2]}_{r,0}}\right)\left(\prod_{j=1}^{i-1}\frac{Z_{r,2j-1}}{R_{L,2j-1} + r_{2j-1} + Z_{r,2j-1}}\right)\left(\frac{R_{L,2i-1}}{R_{L,2i-1} + r_{2i-1} + Z_{r,2i-1}}\right) \\
&= \left(\frac{\tilde{\zeta}_1 - 1}{\tilde{\zeta}_1 + \tilde{\zeta}_2 - 1}\right)\left(\prod_{j=2}^{i}\frac{\tilde{\zeta}_{2j-1} - 1}{\tilde{\zeta}_{2j-1}}\right)\left(\frac{\eta_{r,2i-1}}{\tilde{\zeta}_{2i+1}}\right), \text{ for } i \in \left\{1, 2, \ldots, \frac{N}{2}\right\} \qquad (28) \\
\eta_{2i} &= \left(\frac{Z^{[2]}_{r,0}}{r_0 + Z^{[1]}_{r,0} + Z^{[2]}_{r,0}}\right)\left(\prod_{j=1}^{i-1}\frac{Z_{r,2j}}{R_{L,2j} + r_{2j} + Z_{r,2j}}\right)\left(\frac{R_{L,2i}}{R_{L,2i} + r_{2i} + Z_{r,2i}}\right) \\
&= \left(\frac{\tilde{\zeta}_2 - 1}{\tilde{\zeta}_1 + \tilde{\zeta}_2 - 1}\right)\left(\prod_{j=2}^{i}\frac{\tilde{\zeta}_{2j} - 1}{\tilde{\zeta}_{2j}}\right)\left(\frac{\eta_{r,2i}}{\tilde{\zeta}_{2i+2}}\right), \text{ for } i \in \left\{1, 2, \ldots, \frac{N}{2}\right\} \qquad (29) \\
\eta &= \sum_{i=1}^{\frac{N}{2}}[\eta_{2i-1} + \eta_{2i}] \\
&= \sum_{i=1}^{\frac{N}{2}}\left[\left(\frac{\tilde{\zeta}_1 - 1}{\tilde{\zeta}_1 + \tilde{\zeta}_2 - 1}\right)\left(\prod_{j=2}^{i}\frac{\tilde{\zeta}_{2j-1} - 1}{\tilde{\zeta}_{2j-1}}\right)\left(\frac{\eta_{r,2i-1}}{\tilde{\zeta}_{2i+1}}\right) + \left(\frac{\tilde{\zeta}_2 - 1}{\tilde{\zeta}_1 + \tilde{\zeta}_2 - 1}\right)\left(\prod_{j=2}^{i}\frac{\tilde{\zeta}_{2j} - 1}{\tilde{\zeta}_{2j}}\right)\left(\frac{\eta_{r,2i}}{\tilde{\zeta}_{2i+2}}\right)\right] \qquad (30)
\end{aligned}$$

$$\eta = \sum_{i=1}^{\frac{N}{2}}\left[\left(\frac{\zeta_1 - 1}{\zeta_1 + \zeta_2 - 1}\right)\left(\prod_{j=2}^{i}\frac{\zeta_{2j-1} - 1}{\zeta_{2j-1}}\right)\left(\frac{\eta_{r,2i-1}}{\zeta_{2i+1}}\right) + \left(\frac{\zeta_2 - 1}{\zeta_1 + \zeta_2 - 1}\right)\left(\prod_{j=2}^{i}\frac{\zeta_{2j} - 1}{\zeta_{2j}}\right)\left(\frac{\eta_{r,2i}}{\zeta_{2i+2}}\right)\right] \tag{32}$$

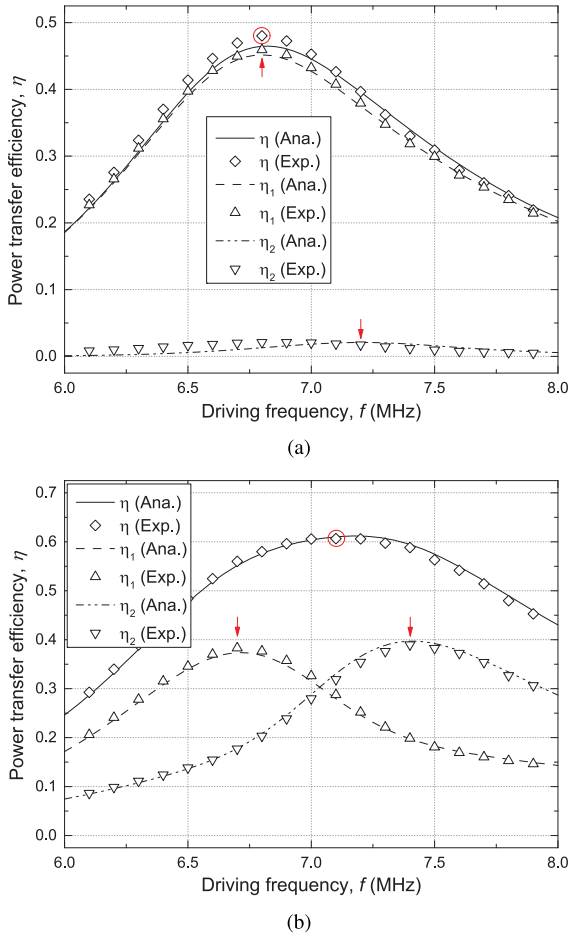

Fig. 4. PTE (η) versus driving frequency (f). (a) Tx–Rx–Rx when $d_{01} = d_{12} = 30$ cm. (b) Rx–Tx–Rx when $d_{01} = d_{02} = 30$ cm.

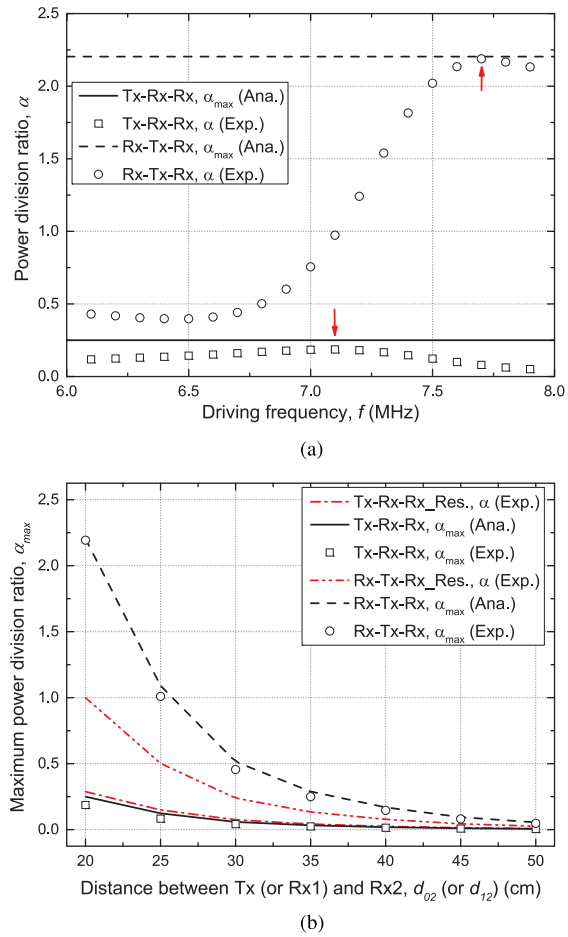

Fig. 5. Performance evaluations for the power division ratio (α). (a) α versus f when $d_{01} = d_{02} = d_{12} = 20$ cm. (b) $\alpha_{\max}$ versus d_{02} (or d_{12}) when $d_{01} = 20$ cm.

that the results of the analysis are in good agreement with the experimental data for both configurations.

Fig. 5 shows the performance evaluations for the power division ratio (α); (a) α versus the driving frequency, f, when $d_{01} = d_{02} = d_{12} = 20$ cm and (b) the maximum power division ratio, $\alpha_{\max}$, versus the distance between Tx (or Rx 1) and Rx 2, d_{02} (or d_{12}), when $d_{01} = 20$ cm for both configurations. In subfigure (a), the value of $\alpha_{\max}$ for Tx–Rx–Rx is 0.19 observed by the experiment near the resonant frequency of Rx 2, e.g., $f = 7.1$ MHz, which corresponds to our analysis. The value of $\alpha_{\max}$ for Rx–Tx–Rx is 2.19, found by the experiment at $f = 7.7$ MHz. Note that α is determined by the ratio of $k_{01}^2 Q_1 F_1^2 \eta_{r,1}$ to $k_{02}^2 Q_2 F_2^2 \eta_{r,2}$ in Rx–Tx–Rx, while α is dominantly influenced by $k_{12}^2 Q_1 Q_2 F_2^2$ rather than the ratio of $\eta_{r,1}$ to $\eta_{r,2}$ in Tx–Rx–Rx. Therefore, the range over which α varies is much wider for Rx–Tx–Rx than for Tx–Rx–Rx. Moreover, the values of $\alpha_{\max}$ found by experiments do not exceed the values of $\alpha_{\max}$ derived by analysis, for both configurations. In subfigure (b), Tx-Rx-Rx_Res and Rx-Tx-Rx_Res indicate the experimental results for the magnetic-resonant WPT, where the resonant frequencies of all resonators are the same as the driving frequency, such that $f = f_0 = f_1 = f_2 = 6.78$ MHz. We note that $\alpha_{\max}$ decreases as d_{02} (or d_{12}) increases because it is difficult to transfer more power to an Rx that is further away, for both configurations. Given that a larger $\alpha_{\max}$ can be achieved in Rx–Tx–Rx than in Tx–Rx–Rx, we confirm that an adjustable power division is more appropriate for an Rx–Tx–Rx configuration. In addition, $\alpha_{\max}$ for Rx–Tx–Rx is much larger than that for Rx–Tx–Rx_Res; thus, the frequency-selective WPT where $f \neq f_0 \neq f_1 \neq f_2$ is more advantageous in terms of power division among Rxs than the magnetic-resonant WPT where $f = f_0 = f_1 = f_2$ in the Rx–Tx–Rx configuration.

Fig. 6 shows the performance evaluations against the position of the resonators; (a) the achievable PTE, $\eta_{\max}$, versus the end-to-end distance, D, when $d_{01} = d_{02} = d_{12}$ and (b) $\eta_{\max}$ versus the distance between Tx and Rx 1, d_{01}, when $D = 80$ cm for both configurations.[3] Subfigure (a) shows the performances when the resonators are equally distributed. The $\eta_{\max}$ of all methods decreases as D increases because the coupling strength

[3]The achievable PTE can be further improved by designing resonators to have larger self-inductance (L_i) and smaller parasitic resistance (r_i) with the optimal load resistance ($R_{L,i}$) [6]–[8] or finding the optimal configuration of resonators to optimize the coupling coefficient (k_{ij}) [13], [18], [24], but in this article, we assume that these parameters are fixed and focus on the effect of the frequency selectivity on the WPT.

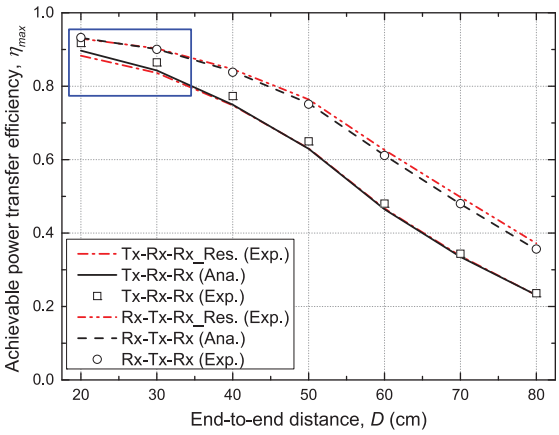

(a)

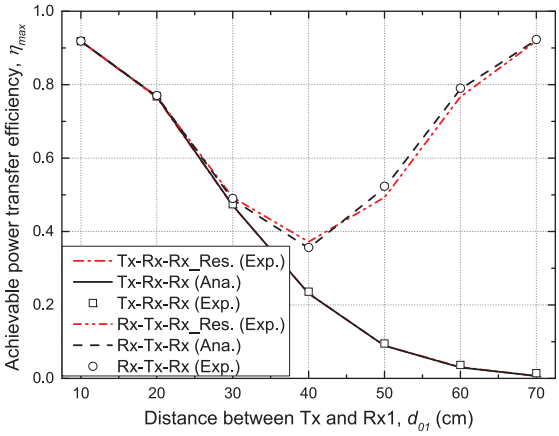

(b)

Fig. 6. Performance evaluations against the position of the resonators. (a) $\eta_{\max}$ versus D when $d_{01} = d_{02} = d_{12}$. (b) $\eta_{\max}$ versus d_{01} when $D = 80$ cm.

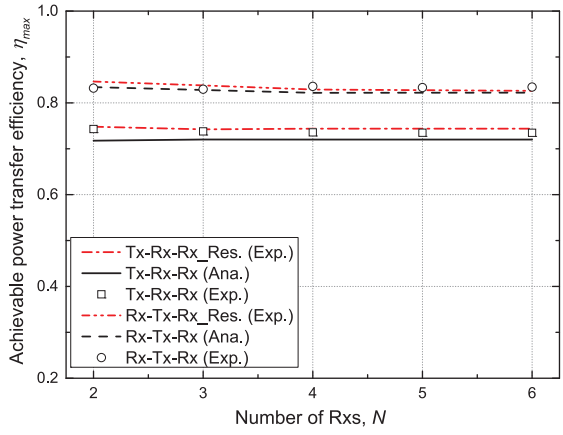

(a)

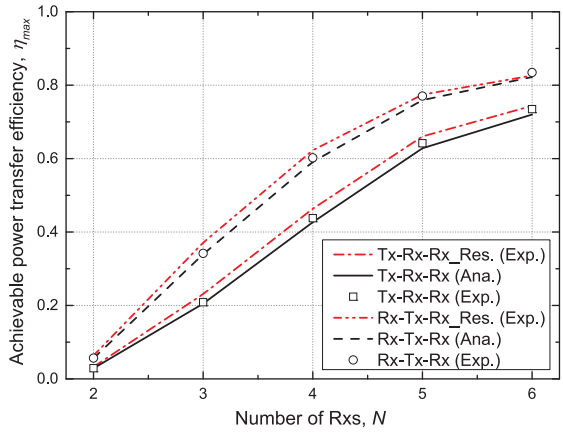

(b)

Fig. 7. Performance evaluations for an increasing number of Rxs (N). (a) $\eta_{\max}$ versus N when $d_{ij} = 20$ cm. (b) $\eta_{\max}$ versus N when $d_{ij} = \frac{D}{N}$ cm and $D = 120$ cm.

between adjacent resonators weakens. Note that Rx–Tx–Rx achieves a higher $\eta_{\max}$ because the Rxs receive power from Tx over a shorter distance, compared to Tx–Rx–Rx. Furthermore, Tx–Rx–Rx has a higher $\eta_{\max}$ than Tx–Rx–Rx_Res at short D, e.g., $D < 40$ cm, as shown in the blue box. This indicates that at short distances, the frequency-selective WPT is preferable to the magnetic-resonant WPT where $f = f_0 = f_1 = f_2$ in the Tx–Rx–Rx configuration, in terms of maximizing the achievable PTE. Subfigure (b) shows the performance for the asymmetric placement of resonators. The $\eta_{\max}$ decreases as d_{01} increases in Tx–Rx–Rx because the nearer Rx is far from Tx. On the other hand, $\eta_{\max}$ is minimized when Tx is placed half way between the Rxs, while $\eta_{\max}$ increases as Tx is moved toward one of the Rxs in Rx–Tx–Rx.

Fig. 7 shows the performance evaluations for an increasing number of Rxs (N). Here, we set the resonant frequencies of the resonators as follows; $f_0 = 6.28$ MHz, $f_1 = 6.28$ MHz, $f_2 = 6.48$ MHz, $f_3 = 6.68$ MHz, $f_4 = 6.88$ MHz, $f_5 = 7.08$ MHz, and $f_6 = 7.28$ MHz. With increasing N, Rx was added in the experiments in the order described in Fig. 2. Subfigure (a) shows $\eta_{\max}$ versus N when the distance between adjacent resonators i and j is set to 20 cm, e.g., $d_{ij} = 20$ cm. As mentioned for the previous results, most of the power tends to be transferred to the nearest Rx, therefore, the addition of further Rxs has little effect in terms of improving the achievable PTE. As a result, $\eta_{\max}$ for all methods is maintained at a relatively constant value even as N increases. Subfigure (b) shows $\eta_{\max}$ versus N when the distance between adjacent resonators varies with increasing N, such that $d_{ij} = \frac{D}{N}$ cm and $D = 120$ cm. As N increases, the Rxs can receive more power from Tx because d_{ij} decreases. As a result, the $\eta_{\max}$ for all the methods can be improved significantly. These results confirm that our analysis results match the experimental results for the WPT system with N Rxs quite well.

Table I shows the performance comparison between the proposed (Prop.) schemes and the conventional (Conv.) schemes when $N = 2$ and $d_{01} = d_{02} = d_{12} = 20$ cm. We choose the schemes in [20] and [22] as comparative schemes for Tx–Rx–Rx and Rx–Tx–Rx configurations, respectively. Note that the proposed schemes use the frequency selectivity for power distribution while the schemes in [20] and [22] adjust load

TABLE I
PERFORMANCE COMPARISON

Config.	Power dist. ($\alpha_{\max}$)		PTE at $\alpha_{\max}$	
Tx-Rx-Rx	Conv. [22]	Prop.	Conv. [22]	Prop.
	1	0.25	0.38	0.68
Rx-Tx-Rx	Conv. [20]	Prop.	Conv. [20]	Prop.
	2.8 (2.2)	2.2	0.56 (0.75)	0.81

resistance to distribute power to Rxs. For fair comparison, the optimal loads are applied to Rxs equidistant from the transmitter for the scheme in [22]. In the Tx–Rx–Rx configuration, the Conv. scheme in [22] transmits the same power to all Rxs, i.e., $\alpha_{\max} = 1$, therefore, it shows better performance in power distribution than the Prop. scheme. However, it experiences a serious degradation in the PTE, compared to the Prop. scheme. Similarly, in the Rx–Tx–Rx configuration, the Conv. scheme in [20] achieves higher $\alpha_{\max}$ but lower PTE than the Prop. scheme. Even at $\alpha = 2.2$ which is the same as $\alpha_{\max}$ of the Prop. scheme, the PTE of the Conv. scheme in [20] is only 0.75 but that of the Prop. scheme is 0.81. This result shows that the frequency selective WPT enables power distribution while guaranteeing higher PTE, compared to the previous works [20] and [22] that adjust the load resistance.

In summary, from the facts that magnetic-resonant WPT is inherently vulnerable to power distribution, compared to the frequency-selective WPT, in the Rx–Tx–Rx configuration and the achievable PTE of the frequency-selective WPT is comparable to that of the magnetic-resonant WPT in both Tx–Rx–Rx and Rx–Tx–Rx configurations, we can conclude that the frequency-selective WPT allows a more adaptive power distribution than the magnetic-resonant WPT with maintaining the achievable PTE in a similar level.

V. CONCLUSION

We have described an analysis of the achievable PTE and power distribution for the frequency-selective WPT with multiple Rx for two different configurations, Tx–Rx–Rx and Rx–Tx–Rx. We considered multiple receivers with different resonant frequencies, and used an ECM to derive the recursive-form equation of the PTE and the power division ratio in terms of the variation in driving frequency. These results allow us to show that the adaptive selection of the driving frequency can improve the system performance, compared with magnetic-resonant WPT where the resonant frequencies of all receivers are the same as the driving frequency. In particular, the frequency-selective WPT is preferable for enabling adaptive power distribution among receivers than the magnetic-resonant WPT in an Rx–Tx–Rx configuration. In addition, the frequency-selective WPT allows higher achievable PTE than the magnetic-resonant WPT over short distances in the Tx–Rx–Rx configuration. By means of experimental verification carried out under a diversity of scenarios, we have demonstrated both the accuracy of our analysis and its theoretical interpretation. We expect that the frequency-selective WPT will receive a lot of attention as an alternative means of enhancing not just the system efficiency but also receiver fairness in the midrange WPT with multiple Rx and can be widely applied to practical applications such as wireless sensor networks, home appliances, and stationary industrial machines. In future work, we will implement a novel WPT system with multiple Rx based on our work to evaluate the performance of real power transmission.

REFERENCES

[1] N. Tesla, "Apparatus for transmitting electrical energy," U.S. Patent 1 119 732, Dec. 1914.

[2] A. Kurs, A. Karalis, R.Moffatt, J. D. Joannopoulos, P. Fisher, and M. Soljacic, "Wireless power transfer via strongly coupled magnetic resonances," *Sci. Express*, vol. 317, no. 5834, pp. 83–86, Jul. 2007.

[3] A. Karalis, J. Joannopoulos, and M. Soljacic, "Efficient wireless nonradiative mid-range energy transfer," *Ann. Phys.*, vol. 323, no. 1, pp. 34–48, Jan. 2008.

[4] S. Cheon, Y. Kim, S. Kang, M. Lee, J. Lee, and T. Zyung, "Circuit-model-based analysis of a wireless energy-transfer system via coupled magnetic resonances," *IEEE Trans. Ind. Electron.*, vol. 58, no. 7, pp. 2906–2914, Jul. 2011.

[5] M. Kiani and M. Ghovanloo, "The circuit theory behind coupled-mode magnetic resonance-based wireless power transmission," *IEEE Trans. Circuits Syst. I*, vol. 59, no. 9, pp. 2065–2074, Sep. 2012.

[6] J. Kim *et al.*, "Coil design and shielding methods for a magnetic resonant wireless power transfer system," *Proc. IEEE*, vol. 101, no. 6, pp. 1332–1342, Jun. 2013.

[7] S. Moon, B. Kim, S. Cho, C. Ahn, and G. Moon, "Analysis and design of a wireless power transfer system with an intermediate coil for high efficiency," *IEEE Trans. Ind. Electron.*, vol. 61, no. 11, pp. 5861–5870, Nov. 2014

[8] X. Zhang, Z. Yuan, Q. Yang, Y. Li, J. Zhu, and Y. Li, "Coil design and efficiency analysis for dynamic wireless charging system for electric vehicles," *IEEE Trans. Magn.*, vol. 52, no. 7, pp. 1–4, Jul. 2016.

[9] I. J. Yoon and H. Ling, "Investigation of near-field wireless power transfer under multiple transmitters," *IEEE Antennas Wireless Propag. Lett.*, vol. 10, pp. 662–665, 2011.

[10] K. Lee and D.-H. Cho, "Diversity analysis of multiple transmitters in wireless power transfer system," *IEEE Trans. Magn.*, vol. 49, no. 6, pp. 2946–2952, Jun. 2013.

[11] R. Johari, J. V. Krogmeier, and D. J. Love, "Analysis and practical considerations in implementing multiple transmitters for wireless power transfer via coupled magnetic resonance," *IEEE Trans. Ind. Electron.*, vol. 61, no. 4, pp. 1774–1783, Apr. 2014.

[12] S. Huh and D. Ahn, "Two-transmitter wireless power transfer with optimal activation and current selection of transmitters," *IEEE Trans. Power Electron.*, vol. 33, no. 6, pp. 4957–4967, Jun. 2018.

[13] J. W. Kim, H. C. Son, K. H. Kim, and Y. J. Park, "Efficiency analysis of magnetic resonance wireless power transfer with intermediate resonant coil," *IEEE Antennas Wireless Propag. Lett.*, vol. 10, pp. 389–392, 2011.

[14] C. K. Lee, W. X. Zhong, and S. Y. R. Hui, "Effects of magnetic coupling of non-adjacent resonators on wireless power domino-resonator systems," *IEEE Trans. Power Electron.*, vol. 27, no. 4, pp. 1905–1916, Apr. 2012.

[15] J. Lee, K. Lee, and D.-H. Cho, "Stability improvement of transmission efficiency based on a relay resonator in a wireless power transfer system," *IEEE Trans. Power Electron.*, vol. 32, no. 5, pp. 3297–3300, May 2017.

[16] D. Ahn and S. Hong, "A study on magnetic field repeater in wireless power transfer," *IEEE Trans. Ind. Electron.*, vol. 60, no. 1, pp. 360–371, Jan. 2013.

[17] W. X. Zhong, C. K. Lee, and S. Y. R. Hui, "General analysis on the use of Tesla's resonators in domino forms for wireless power transfer," *IEEE Trans. Ind. Electron.*, vol. 60, no. 1, pp. 261–270, Jan. 2013.

[18] K. Lee and S. H. Chae, "Effect of quality factor on determining the optimal position of a transmitter in wireless power transfer using a relay," *IEEE Microw. Wireless Compon. Lett.*, vol. 27, no. 5, pp. 521–523, May 2017.

[19] A. Kurus, R. Moffatt, and M. Soljacic, "Simultaneous mid-range power transfer to multiple devices," *Appl. Phys. Lett.*, vol. 96, no. 4, pp. 1–4, Jan. 2010.

[20] K. Lee and D.-H. Cho, "Analysis of wireless power transfer for adjustable power distribution among multiple receivers," *IEEE Antennas Wireless Propag. Lett.*, vol. 14, pp. 950–953, 2015.

[21] M. Fu, T. Zhang, C. Ma, and X. Zhu, "Efficiency and optimal loads analysis for multiple-receiver wireless power transfer systems," *IEEE Trans. Microw. Theory Technol.*, vol. 63, no. 3, pp. 801–812, Mar. 2015.
[22] Y. Zhang, Z. Zhao, K. Chen, F. He, and L. Yuan, "Wireless power transfer to multiple loads over various distances using relay resonators," *IEEE Microw. Wireless Compon. Lett.*, vol. 25, no. 5, pp. 337–339, May 2015.
[23] M. Fu, T. Zhang, X. Zhu, P. C.-K. Luk, and C. Ma, "Compensation of cross coupling in multiple-receiver wireless power transfer systems," *IEEE Trans. Ind. Inform.*, vol. 12, no. 2, pp. 474–482, Jan. 2016.
[24] K. Lee and S. H. Chae, "Power transfer efficiency analysis of intermediate-resonator for wireless power transfer," *IEEE Trans. Power Electron.*, vol. 33, no. 3, pp. 2484–2493, Mar. 2018.
[25] A. P. Sample, D. A. Meyer, and J. R. Smith, "Analysis, experimental results, and range adaptation of magnetically coupled resonators for wireless power transfer," *IEEE Trans. Ind. Electron.*, vol. 58, no. 2, pp. 544–554, Feb. 2011.
[26] W.-S. Lee, W.-I. Son, K.-S. Oh, and J.-W. Yu, "Contactless energy transfer systems using antiparallel resonant loops," *IEEE Trans. Ind. Electron.*, vol. 60, no. 1, pp. 350–359, Jan. 2013.
[27] W.-Q. Niu, J.-X. Chu, W. Gu, and A.-D. Shen, "Exact analysis of frequency splitting phenomena of contactless power transfer systems," *IEEE Trans. Circuits Syst. I., Reg. Papers*, vol. 60, no. 6, pp. 1670–1677, Jun. 2013.
[28] Y. Zhang and Z. Zhao, "Frequency splitting analysis of two-coil resonant wireless power transfer," *IEEE Antennas Wireless Propag. Lett.*, vol. 13, pp. 400–402, 2014.
[29] W.-K. Choi, C.-W. Park, and K. Lee, "Circuit analysis of achievable transmission efficiency in an overcoupled region for wireless power transfer systems," *IEEE Syst. J.*, vol. 12, no. 4, pp. 3873–3876, Mar. 2014.
[30] Y. Zhang, Z. Zhao, and K. Chen, "Frequency decrease analysis of resonant wireless power transfer," *IEEE Trans. Power Electron.*, vol. 29, no. 3, pp. 1058–1063, Mar. 2014.
[31] D. Ahn, "Transmitter coil resonant frequency selection for wireless power transfer," *IEEE Trans. Power Electron.*, vol. 33, no. 6, pp. 5029–5041, Jun. 2018.
[32] B. L. Cannon, J. F. Hoburg, D. D. Stancil, and S. C. Goldstein, "Magnetic resonant coupling as a potential means for wireless power transfer to multiple small receivers," *IEEE Trans. Power Electron.*, vol. 24, no. 7, pp. 1819–1825, Jul. 2009.
[33] D. Ahn and S. Hong, "Effect of coupling between multiple transmitters or multiple receivers on wireless power transfer," *IEEE Trans. Ind. Electron.*, vol. 60, no. 7, pp. 2602–2613, Jul. 2013.
[34] W. Zhong and S. Y. R. Hui, "Auxiliary circuits for power flow control in multifrequency wireless power transfer systems with multiple receivers," *IEEE Trans. Power Electron.*, vol. 30, no. 10, pp. 5902–5910, Oct. 2015.
[35] Y. Zhang, T. Lu, Z. Zhao, F. He, K. Chen, and L. Yuan, "Selective wireless power transfer to multiple loads using receivers of different resonant frequencies," *IEEE Trans. Power Electron.*, vol. 30, no. 11, pp. 6001–6005, Nov. 2015.
[36] D. Ahn and P. P. Mercier, "Wireless power transfer with concurrent 200 kHz and 6.78 MHz operation in a single transmitter device," *IEEE Trans. Power Electron.*, vol. 31, no. 7, pp. 5018–5029, Jul. 2016.
[37] K. Fotopoulou and B. W. Flynn, "Wireless power transfer in loosely coupled links: Coil misalignment model," *IEEE Trans. Magn.*, vol. 47, no. 2, pp. 416–430, Feb. 2011.
[38] K. Lee and D.-H. Cho, "Maximizing the capacity of magnetic induction communication for embedded sensor networks in strongly and loosely coupled regions," *IEEE Trans. Magn.*, vol. 49, no. 9, pp. 5055–5062, Sep. 2013.

Kisong Lee (S'10–M'14) received the B.S., M.S., and Ph.D. degrees in electrical engineering from the Korea Advanced Institute of Science and Technology, Daejeon, South Korea, in 2007, 2009, and 2013, respectively.

He was a Researcher with the Electronics and Telecommunications Research Institute from September 2013 to February 2015. From March 2015 to August 2017, he was an Assistant Professor with the Department of Information and Telecommunication Engineering, Kunsan National University. He is currently an Associate Professor with the School of Information and Communication Engineering, Chungbuk National University, Cheongju, South Korea. His research interests include system optimization, wireless power transfer, energy harvesting networks, information security, and deep learning.

Sung Ho Chae (S'08–M'14) received the B.S., M.S., and Ph.D. degrees in electrical engineering from the Korea Advanced Institute of Science and Technology, Daejeon, South Korea, in 2005, 2008, and 2013, respectively.

From August 2013 to January 2018, he was with Samsung Electronics, Suwon, South Korea, as a Senior Engineer. From March 2018 to August 2019, he was an Assistant Professor with the Department of Electrical Engineering, Chosun University, Gwangju, South Korea. He has been an Assistant Professor with the Department of Electronic Engineering, Kwangwoon University, Seoul, South Korea, since September 2019. His research interests include network information theory, antenna theory, and communication theory.